Organometallics | 3b2 | ver.9 | 12/11/09 | 22:5 | Msc: om-2009-00750t | TEID: deb00 | BATID: 00000 | Pages: 8.17

ORGANOMETALLICS
Article

Organometallics **XXXX,** *XXX,* 000–000 A
DOI: 10.1021/om900750t

Infrared Spectra of Small Insertion and Methylidene Complexes in Reactions of Laser-Ablated Palladium Atoms with Halomethanes

Han-Gook Cho,[†] Lester Andrews,*[,‡] Bess Vlaisavljevich,[§] and Laura Gagliardi[§,⊥]

[†]*Department of Chemistry, University of Incheon, 177 Dohwa-dong, Nam-ku, Incheon, 402-749, South Korea,* [‡]*Department of Chemistry, University of Virginia, P.O. Box 400319, Charlottesville, Virginia 22904-4319,* [§]*Department of Chemistry, University of Minnesota, 207 Pleasant St. SE Minneapolis, Minnesota 55455-0431, and* [⊥]*Department of Physical Chemistry, University of Geneva, 30, q. E. Ansermet, 1211 Genève, Switzerland*

Received August 27, 2009

Palladium carbene complexes, $CX_2{=}PdX_2$, are prepared along with the insertion products, $CX_3{-}PdX$, in reactions of laser-ablated Pd atoms with tetrahalomethanes and identified from matrix infrared spectra and density functional frequency calculations. The carbon−metal bonds of the $CCl_2{=}PdCl_2$ and $CClF{=}PdCl_2$ complexes are essentially double bonds with effective bond orders of 1.9, near those for the Pt and Ni analogues, as calculated by CASPT2 methods. On the other hand, only insertion complexes are generated from mono-, di-, and trihalomethane precursors. While the carbenes have staggered allene-type structures, many insertion complexes containing C−Cl bonds reveal distinct bridged structures, which indicate effective coordination of Cl to the metal center.

Introduction

Numerous high-oxidation-state complexes are an essential part of coordination chemistry, and they help to understand the nature of carbon−transition metal bonding interactions.[1,2] The chemistry of these complexes includes synthetic processes such as metathesis, catalysis, and C−H insertion.[3] The structures and photochemical properties of such complexes have been explored by theoretical methods[4a,b] and in particular the oxidative insertion of Pd into the $CH_3{-}X$ bond.[4c]

Laser ablation/matrix isolation spectroscopy has been used recently to prepare small high-oxidation-state complexes from group 3−8 transition and actinide metal reactions with halomethanes and small alkanes through C−H(X) insertion and subsequent H(X) migration.[5−9] These complexes show distinct structures, particularly due to agostic interaction, and photoreversibility. Their small numbers of atoms make them ideal for high-level theoretical analysis, and they are good model systems of larger ligand stabilized complexes. Higher-oxidation-state complexes, however, are less important for the later transition metals in the periodic table because the d-orbitals are more completely filled.

Small Pt carbene complexes and the related insertion products have subsequently been identified as products of reactions with methane and halomethanes.[10] The small Pt methylidenes have a substantial amount of double-bond character from $d_\pi{-}p_\pi$ bonding, and their C−Pt bonds are considerably shorter than those of typical Pt(II) carbene complexes. It appears that the small Pt methylidene complexes have substantial Pt(IV) character.[11] In contrast, the corresponding nickel complexes reveal essentially single C−Ni bonds.[12] Finally, Pt is a very effective C−H insertion

*To whom correspondence should be addressed. E-mail: lsa@virginia.edu.

(1) (a) Fischer, E. O.; Kreis, G.; Kreiter, C. G.; Müller, J.; Huttner, G.; Lorenz, H. *Angew. Chem., Int. Ed. Engl.* **1973**, *12*, 564. (b) Schrock, R. R. *J. Am. Chem. Soc.* **1974**, *96*, 6796. (c) Shaefer, H. F. III. *Acc. Chem. Res.* **1977**, *10*, 287.

(2) (a) Herndon, J. W. *Coord. Chem. Rev.* **2009**, *253*, 1517. (b) Herndon, J. W. *Coord. Chem. Rev.* **2009**, *253*, 86. (c) Herndon, J. W. *Coord. Chem. Rev.* **2007**, *251*, 1158. (d) Herndon, J. W. *Coord. Chem. Rev.* **2006**, *250*, 1889. (e) Herndon, J. W. *Coord. Chem. Rev.* **2005**, *249*, 999. (f) Herndon, J. W. *Coord. Chem. Rev.* **2004**, *248*, 3, and earlier review articles in this series.

(3) (a) Crabtree, R. H. *Chem. Rev.* **1995**, *95*, 987, and references therein. (b) Ujaque, G.; Cooper, A. C.; Maseras, F.; Eisenstein, O.; Caulton, K. G. *J. Am. Chem. Soc.* **1998**, *120*, 361. (c) Wada, K.; Craig, B.; Pamplin, C. B.; Legzdins, P; Patrick, B. O.; Tsyba, I.; Bau, R. *J. Am. Chem. Soc.* **2003**, *125*, 7035.

(4) (a) Clot, E.; Eisenstein, O. In *Computational Inorganic Chemistry*; Kaltzoyannis, N., McGrady, J. E., Eds.; Structure and Bonding, Springer: Heidelberg, 2004; pp 1−36. (b) Aubert, C.; Buisine, O.; Malacria, M.; *Chem. Rev.* **2002**, *102*, 813, and references therein. (c) de Jong, G. T.; Bickelhaupt, F. M. *J. Chem. Theory Comput.* **2007**, *3*, 514.

(5) (a) Andrews, L.; Cho, H.-G. *Organometallics* **2006**, *25*, 4040, and references therein (Review article, groups 4−6). (b) Lyon, J. T.; Cho, H.-G.; Andrews, L. *Organometallics* **2007**, *26*, 2519 (Ti, Zr, Hf + CHX_3, CX_4). (c) Lyon, J. T.; Cho, H.-G.; Andrews, L. *Organometallics* **2007**, *26*, 6373 (Cr, Mo, W + CHX_3, CX_4).

(6) (a) Cho, H.-G.; Andrews, L. *J. Phys. Chem. A* **2007**, *111*, 2480. (b) Cho, H.-G.; Andrews, L. *Organometallics* **2007**, *26*, 633 (group 3).

(7) (a) Cho, H.-G.; Andrews, L. *Organometallics* **2007**, *26*, 4096. (b) Cho, H.-G.; Andrews, L. *Inorg. Chem.* **2008**, *47*, 1653 (Re).

(8) (a) Cho, H.-G.; Lyon, J. T.; Andrews, L. *Organometallics* **2008**, *27*, 5241. (b) Cho, H.-G.; Andrews, L. *Eur. J. Inorg. Chem.* **2008**, 2537. (c) Cho, H.-G.; Andrews, L. *Organometallics* **2008**, *27*, 1786 (group 8).

(9) (a) Andrews, L.; Cho, H.-G. *J. Phys. Chem. A* **2005**, *109*, 6796. (b) Cho, H.-G.; Lyon, J. T.; Andrews, L. *J. Phys. Chem. A* **2008**, *112*, 6902. (c) Lyon, J. T.; Cho, H.-G.; Andrews, L. *Eur. J. Inorg. Chem.* **2008**, 1047 (Th, U).

(10) (a) Cho, H.-G.; Andrews, L. *J. Am. Chem. Soc.* **2008**, *130*, 15836. (b) Cho, H.-G.; Andrews, L. *J. Phys. Chem. A* **2008**, *112*, 12293. (c) Cho, H.-G.; Andrews, L. *Organometallics*, **2009**, *28*, 1358 (Pt).

(11) Prokopchuk, E. M.; Puddephatt, R. J. *Organometallics* **2003**, *22*, 563, and references therein (Pt(IV)).

(12) Cho, H.-G.; Andrews, L. *Organometallics* **2009**, 28, in press (Ni).

agent in reactions with acetylene, ethylene, and methane, whereas Pd is not.[13]

Here we complete our investigation of group 10 transition metal complexes and report reactions of Pd atoms with halomethanes. In contrast to the case of Pt,[10] which is considered the most effective C−H insertion agent among group 10 metals,[10,12] only tetrahalomethanes generate Pd methylidenes. The identified products also have interesting structures, particularly due to intermolecular interaction between X bonded to C and the metal center.

Experimental and Computational Methods

Laser-ablated palladium atoms were reacted as described previously[10,13,14] with argon-diluted samples of CCl_4 (Fisher), $^{13}CCl_4$ (90% enriched, MSD Isotopes), $CFCl_3$, CF_2Cl_2 (Dupont), $CHCl_3$, CH_2Cl_2, CH_2FCl, CH_2F_2 (Dupont), $CDCl_3$, CD_2Cl_2, CD_2FCl, and CD_2F_2 (synthesized in this laboratory[14c]) during condensation at 10 K using a closed-cycle refrigerator (Air Products Displex). Reagent gas mixtures ranged 0.2−1.0% in argon. The Nd:YAG laser fundamental (1064 nm, 10 Hz repetition rate, 10 ns pulse width) was focused on a rotating Pd metal target (Johnson Matthey) using a 5−20 mJ/pulse. After initial reaction, infrared spectra were recorded at a resolution of 0.5 cm^{-1} using a Nicolet 550 spectrometer with a Hg−Cd−Te range B detector. Samples were later irradiated for 20 min periods by a mercury arc street lamp (175 W, globe removed) using a combination of optical filters and subsequently annealed to allow further reagent diffusion.

In order to provide support for the assignment of new experimental frequencies and to correlate with related works,[5−10] density functional theory (DFT) calculations were performed using the Gaussian 03 program system,[15] the B3LYP density functional,[16] the 6-311++G(3df,3pd) basis sets for H, C, F, and Cl,[17] and the SDD pseudopotential and basis set[18] for Pd to provide vibrational frequencies for the reaction products. Geometries were fully relaxed during optimization, and the optimized geometry was confirmed by vibrational analysis. The BPW91[19] functional was also employed to complement the B3LYP results. The vibrational frequencies were calculated analytically, and zero-point energy is included in the calculation of binding and reaction energies. Previous investigations have shown that DFT-calculated harmonic frequencies are usually slightly higher than observed frequencies,[5−10,20] and they provide useful estimates for infrared spectra of new molecules. Bonding in the carbene products was examined using CASSCF/CASPT2 methods and triple-ζ (ANO-RCC-VTZP) basis sets.[21] An active space of (6,6) was chosen for the orbitals involved in the C−M bonds. A CASPT2 geometry optimization was performed for the carbenes starting from DFT geometries. The orbitals shown below and the occupation numbers used to compute the effective bond orders (EBO = bonding minus antibonding electons divided by 2) are from the final CASPT2 calculation at the optimized geometry. The CASSCF/CASPT2 calculations were performed using the Molcas 7.4 software.[22]

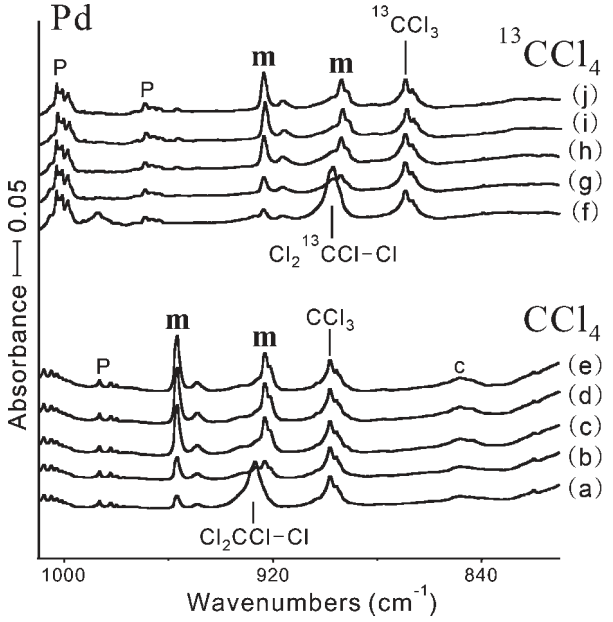

Figure 1. Infrared spectra in the 1010−810 cm^{-1} region for the laser-ablated palladium atom and carbon tetrachloride reaction products in excess argon at 10 K. (a) Pd and CCl_4 (0.5% in argon) co-deposited for 1 h, (b) as (a) after visible ($\lambda > 420$ nm) irradiation, (c) as (b) after ultraviolet (240−380 nm) irradiation, (d) as (c) after full arc ($\lambda > 220$ nm) irradiation, and (e) as (d) after annealing to 26 K. (f) Pd and $^{13}CCl_4$ (0.5% in argon, 90% enriched) co-deposited for 1 h, (g) as (f) after visible irradiation, (h) as (g) after UV (240−380 nm) irradiation, (i) as (h) after full arc irradiation, (j) as (i) after annealing to 26 K. **m**, P, and c stand for product, precursor, and common absorptions, respectively.

Results and Discussion

Reactions of palladium atoms with halomethanes were investigated, and infrared spectra and density functional frequency calculations of the products will be presented in turn.

(13) (a) Wang, X.; Andrews, L. *J. Phys. Chem. A* **2004**, *108*, 4838. (b) Cho, H.-G.; Andrews, L. *J. Phys. Chem. A* **2004**, *108*, 6272.

(14) (a) Andrews, L.; Citra, A. *Chem. Rev.* **2002**, *102*, 885, and references therein. (b) Andrews, L. *Chem. Soc. Rev.* **2004**, *33*, 123, and references therein. (c) Isotopic modifications synthesized: see: Andrews, L.; Willner, H.; Prochaska, F. T. *J. Fluorine Chem.* **1979**, *13*, 273.

(15) Frisch, M. J.; Trucks, G. W.; Schlegel, H. B.; Scuseria, G. E.; Robb, M. A.; Cheeseman, J. R.; Montgomery, J. A. Jr.; Vreven, T.; Kudin, K. N.; Burant, J. C.; Millam, J. M.; Iyengar, S. S.; Tomasi, J.; Barone, V.; Mennucci, B.; Cossi, M.; Scalmani, G.; Rega, N.; Petersson, G. A.; Nakatsuji, H.; Hada, M.; Ehara, M.; Toyota, K.; Fukuda, R.; Hasegawa, J.; Ishida, M.; Nakajima, T.; Honda, Y.; Kitao, O.; Nakai, H.; Klene, M.; Li, X.; Knox, J. E.; Hratchian, H. P.; Cross, J. B.; Adamo, C.; Jaramillo, J.; Gomperts, R.; Stratmann, R. E.; Yazyev, O.; Austin, A. J.; Cammi, R.; Pomelli, C.; Ochterski, J. W.; Ayala, P. Y.; Morokuma, K.; Voth, G. A.; Salvador, P.; Dannenberg, J. J.; Zakrzewski, V. G.; Dapprich, S.; Daniels, A. D.; Strain, M. C.; Farkas, O.; Malick, D. K.; Rabuck, A. D.; Raghavachari, K.; Foresman, J. B.; Ortiz, J. V.; Cui, Q.; Baboul, A. G.; Clifford, S.; Cioslowski, J.; Stefanov, B. B.; Liu, G.; Liashenko, A.; Piskorz, P.; Komaromi, I.; Martin, R. L.; Fox, D. J.; Keith, T.; Al-Laham, M. A.; Peng, C. Y.; Nanayakkara, A.; Challacombe, M.; Gill, P. M. W.; Johnson, B.; Chen, W.; Wong, M. W.; Gonzalez, C.; Pople, J. A. *Gaussian 03*, Revision C.02; Gaussian, Inc.: Wallingford, CT, 2004.

(16) (a) Becke, A. D. *J. Chem. Phys.* **1993**, *98*, 5648. (b) Lee, C.; Yang, Y.; Parr, R. G. *Phys. Rev. B* **1988**, *37*, 785.

(17) Raghavachari, K.; Trucks, G. W. *J. Chem. Phys.* **1989**, *91*, 1062.

(18) Andrae, D.; Haeussermann, U.; Dolg, M.; Stoll, H.; Preuss, H. *Theor. Chim. Acta* **1990**, *77*, 123.

(19) (a) Becke, A. D. *Phys. Rev. A* **1988**, *38*, 3098. (b) Burke, K.; Perdew, J. P.; Wang, Y. In *Electronic Density Functional Theory: Recent Progress and New Directions*; Dobson, J. F., Vignale, G., Das, M. P. Eds.; Plenum: New York, 1998.

(20) (a) Scott, A. P.; Radom, L. *J. Phys. Chem.* **1996**, *100*, 16502. (b) Andersson, M. P.; Uvdal, P. L. *J. Phys. Chem. A* **2005**, *109*, 3937.

(21) (a) Roos, B. O. The Complete Active Space Self-Consistent Field Method and its Applications in Electronic Structure Calculations. In *Advances in Chemical Physics; Ab Initio Methods in Quantum Chemistry−II*; Lawley, K. P., Ed.; John Wiley & Sons Ltd.: New York, 1987; Chapter 69, p 399. (b) Andersson, K.; Malmqvist, P.-Å.; Roos, B. O. *J. Chem. Phys.* **1992**, *96*, 1218. (c) Roos, B. O.; Lindh, R.; Malmqvist, P.-Å.; Veryazov, V.; Widmark, P.-O. *J. Phys. Chem. A* **2005**, *109*, 6575, triple-ζ (ANO-RCC-VTZP) basis.

(22) Karlström, G.; Lindh, R.; Malmqvist, P.-Å.; Roos, B. O.; Ryde, U.; Veryazov, V.; Widmark, P.-O.; Cossi, M.; Schimmelpfennig, B.; Neogrady, P.; Seijo, L. *Comput. Mater. Sci.* **2003**, *28*, 222.

Table 1. Observed and Calculated Fundamental Frequencies of CCl_2-PdCl_2 Isotopomers in the $^1A_1$ Ground State in C_{2v} Symmetry[a]

approximate description	$^{12}CCl_2-PdCl_2$ obsd[b]	B3LYP[c]	int[c]	BPW91[c]	int[c]	$^{13}CCl_2-PdCl_2$ obsd[b]	B3LYP[c]	int[c]	BPW91[c]	int[c]
A_1 C−Cl_2, Pd−C str.	956.8	949.9	244	943.2	203	923.6	916.3	227	909.7	189
B_2 CCl_2 str.	923.1, 921.1	905.2	214	871.1	197	893.8, 891.6	876.0	200	843.1	184
B_1 $PdCCl_2$ deform		447.2	2	431.9	5		430.9	2	405.8	0
A_1 Pd−C str., CCl_2 bend		440.5	2	421.2	0		439.8	2	431.4	5
B_1 $PdCl_2$ str.		377.8	73	380.5	62		377.8	73	380.4	62
A_1 $PdCl_2$ str.		323.6	4	325.7	7		323.6	4	325.6	7
A_1 $PdCl_2$, CCl_2 bend		230.9	0	226.5	1		230.8	0	226.5	1
B_2 Cl_2CPd deform		199.3	0	194.4	0		198.5	0	193.7	0
B_2 $PdCl_2$ def.		102.3	3	95.9	2		102.2	3	95.8	2
A_1 $PdCl_2$ bend		90.2	1	90.3	0		90.1	1	90.2	0
B_1 $PdCl_2$ rock		60.0	1	62.4	0		60.0	1	62.4	0
A_2 CCl_2 twist		18.7	0	21.5	0		18.7	0	21.5	0

[a] Frequencies and intensities are in cm^{-1} and km/mol. Approximate mode descriptions as considerable mixing is involved. The first and fourth modes differ by phasing of the C motion, antisymmetric for the first and symmetric for the fourth mode. [b] Observed in an argon matrix. Chlorine isotopic splitting listed. [c] Harmonic frequencies and intensities computed with B3LYP or BPW91/6-311+G(3df) basis and the SDD core potential and basis set for Pd.

Pd + CCl_4. Figure 1 shows the spectra from reactions of Pd with CCl_4 and its ^{13}C isotopomers, where the **m** absorptions double on visible photolysis, double again with UV irradiation, and increase 10% more on full arc photolysis (more than 400% increase in total). Two strong **m** absorptions, one at 956.8 cm^{-1} (with a satellite at 949.1 cm^{-1} for a matrix site splitting) and the other at 923.1 cm^{-1} (with a shoulder at 921.1 cm^{-1} for chlorine isotopic splitting), are clearly observed. Their ^{13}C counterparts are observed at 923.6 cm^{-1} (with a satellite at 916.1 cm^{-1}) (12/13 ratio of 1.036) and at 893.8 cm^{-1} (with a shoulder at 891.6 cm^{-1}) (12/13 ratio of 1.033), respectively. As reported for Pt and Ni products, the ^{12}C counterpart at 956.8 cm^{-1} with about 1/10 of the absorbance of the ^{13}C product absorption in the ^{13}C-enriched sample shows that this product contains a single C atom.[10a,12] The 921.1 and 891.6 cm^{-1} shoulders on the 923.1 and 893.8 cm^{-1} bands are 6/9 of the main band absorbances, which is appropriate for natural abundance chlorine isotopes for a species containing two equivalent chlorine atoms (statistical population of one ^{35}Cl and one ^{37}Cl vs two ^{35}Cl atoms). In addition bands at 1036.4 cm^{-1} (CCl_3^+), 1019.3 and 926.7 cm^{-1} (Cl_2CCl-Cl), and 898 cm^{-1} (CCl_3) are common to all laser-ablated metal experiments with CCl_4 owing to the presence of vacuum ultraviolet irradiation in the ablation plume.[23−25] [The chlorine isotopic splitting on the CCl_3 band is not completely resolved in this experiment: this pattern for a degenerate mode has been explained in the literature.[25]]

The 956.8 and 923.1 cm^{-1} absorptions are assigned to the symmetric and antisymmetric CCl_2 stretching modes of the carbene complex, singlet CCl_2PdCl_2. Parallel to the Pt and Ni cases, the symmetric CCl_2 stretching mode is coupled with the C−Pd stretching mode, resulting in a higher frequency than that of the antisymmetric mode and the description as C vibrating between two chlorine and one palladium center. Although a pure symmetric CCl_2 stretching mode would have a lower 12/13 isotopic ratio, the mode coupling with carbon results in more carbon motion than in the antisymmetric mode. The observed frequencies are also compared with the DFT frequencies in Table 1, with good correlation, while the predicted values are again slightly lower, and the observed carbon-13 shifts of 33.2 and 29.3 cm^{-1} are compared with calculated shifts of 33.6 and 29.2 cm^{-1}. The strong CCl_2 stretching absorptions substantiate the formation of CCl_2PdCl_2. The calculated infrared intensities in Table 1 also show that CCl_2PdCl_2 has no other strong observable band in our spectroscopic range. Since the identification of CCl_2PdCl_2 is substantiated by comparison between observed and calculated frequencies, wave function based CASPT2 frequencies are compared with the observed matrix infrared and B3LYP density functional computed frequencies in Table S1 (Supporting Information).

The singlet and triplet states of $CCl_2{=}PdCl_2$ are 47 and 23 kcal/mol more stable than the reactants ($Pd(^1S)$ + CCl_4), whereas the singlet and triplet states of CCl_3-PdCl are

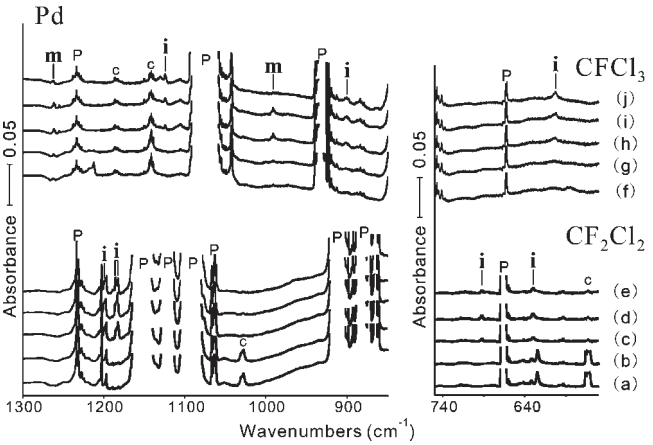

Figure 2. Infrared spectra in the 1300−850 and 750−550 cm^{-1} regions for the reaction products of the laser-ablated palladium atom with CF_2Cl_2 and $CFCl_3$ in excess argon at 10 K. (a) Pd and CF_2Cl_2 reagent (0.5% in argon) co-deposited for 1 h; (b−e) as (a) spectra taken following the irradiation and annealing sequence described in Figure 1 caption (visible, UV, and full arc irradiations and annealing to 26 K). (f) Pd and $CFCl_3$ reagent (0.5% in argon) co-deposited for 1 h; (g−j) as (f) spectra taken following the same irradiation and annealing sequence. **i** and **m** designate the product absorption groups, while P and c stand for the precursor and common absorptions.

(23) (a) Jacox, M. E.; Milligan, D. E. *J. Chem. Phys.* **1971**, *54*, 3935. (b) Jacox, M. E. *Chem. Phys.* **1976**, *12*, 51. (c) Prochaska, F. T.; Andrews, L. *J. Chem. Phys.* **1977**, *67*, 1091 (CCl_3^+).
(24) Maier, G.; Reisenauer, H. P.; Hu, J.; Hess, B. A., Jr.; Schaad, L. J. *Tetrahedron Lett.* **1989**, *30*, 4105 (Cl_2CCl−Cl).
(25) Andrews, L. *J. Chem. Phys.* **1968**, *48*, 972 (CCl_3).

Table 2. Observed and Calculated Fundamental Frequencies of CF_2-PdCl_2 and $CFCl-PdCl_2$ in the ^1A and $^1A'$ Ground States[a]

	CF_2-PdCl_2						$CFCl-PdCl_2$				
approximate description	obsd[b]	B3LYP[c]	int[c]	BPW91[c]	int[c]	approximate description	obsd[b]	B3LYP[c]	int[c]	BPW91[c]	int[c]
A CF_2 sym. str.	n.o.	1324.4	561	1274.6	556	A′ C−F str.	1261.3	1267.4	288	1206.2	287
B CF_2 asym. str.		1307.8	229	1225.8	209	A′ C−Cl str.	991.2	977.5	358	951.9	295
A CF_2 bend		724.4	13	695.1	4	A′ CFCl scis.		536.8	2	523.1	4
B CF_2 wag		558.0	39	526.4	15	A″ CFCl wag		499.7	17	467.8	3
B $PdCl_2$ asym. str.		382.0	71	382.9	59	A″ $PdCl_2$ as. str.		378.9	71	381.8	61
A $PdCl_2$ sym. str.		357.9	0	370.1	2	A′ C−Pd str.		335.3	3	338.6	7
A C−Pd str.		327.2	0	326.2	0	A′ PdCl2 s. str.		321.5	0	318.6	0
B CF_2 rock		286.1	1	283.5	0	A′ CFCl rock		214.4	0	211.3	0
A $PdCl_2$ bend		108.3	4	105.7	2	A′ $PdCl_2$ wag		105.1	3	103.2	2
A $PdCl_2$ wag		96.5	3	92.4	1	A′ $PdCl_2$ scis.		89.2	2	91.1	0
B CCl_2 twist		64.2	1	60.8	0	A″ $PdCl_2$ rock		55.8	0	63.4	0
A $PdCl_2$ rock		31.4	0	19.2	0	A″ CFCl tort.		−12.1	0	20.1	0

[a] Frequencies and intensities are in cm^{-1} and km/mol. [b] Observed in an argon matrix. [c] Frequencies and intensities computed with B3LYP or BPW91/6-311+G(3df) are for harmonic calculations, and the SDD core potential and basis set are used for Pd. CF_2-PdCl_2 has a C_2 structure, whereas $CFCl-PdCl_2$ has a C_s structure.

Table 3. Observed and Calculated Fundamental Frequencies of $CF_2Cl-PdCl$ and $CFCl_2-PdCl$ in the $^1A'$ and ^1A Ground States[a]

	$CF_2Cl-PdCl$						$CFCl_2-PdCl$				
approximate description	obsd[b]	B3LYP[c]	int[c]	BPW91[c]	int[c]	approximate description	obsd[b]	B3LYP[c]	int[c]	BPW91[c]	int[c]
A″ CF_2 sym. str.	1199.0	1195.5	178	1140.7	173	C−F str.	1124.2	1144.1	212	1097.5	222
A′ CF_2 asym. str.	1182.3	1186.9	430	1143.9	447	C−Cl str.	900.4	859.9	261	837.0	290
A′ CF_2 scis.	692.7	695.1	81	669.0	41	C−Cl[d] str.	602.2	597.5	141	551.7	95
A′ C−Cl str.	630.3	626.4	171	589.1	164	$CFCl_2$ deform		487.0	33	469.3	47
A′ Pd−Cl str.		374.8	90	376.8	70	Pd−Cl str.		365.1	66	366.7	56
A″ C−Pd str.		355.0	1	343.7	8	CFCl bend		350.4	0	333.3	7
A′ CF_2 rock		344.5	0	328.1	0	$PdCl_2$ bend		281.1	3	269.8	6
A′ CF_2Cl deform		287.1	7	274.9	13	C−Pd str.		258.4	6	246.5	6
A″ CF_2 rock		212.5	0	202.0	0	CClPd bend		182.5	2	186.9	5
A′ ClCPd bend		183.3	2	189.4	4	CFCl rock		158.6	1	153.9	1
A″ Pd−Cl tort.		77.1	2	80.3	1	PdCl tort.		71.2	2	76.5	1
A′ CPdCl bend		73.6	5	76.4	4	PdCCl bend		64.2	5	66.3	3

[a] Frequencies and intensities are in cm^{-1} and km/mol. [b] Observed in an argon matrix. [c] Frequencies and intensities computed with B3LYP or BPW91/6-311+G(3df) are for harmonic calculations, and the SDD core potential and basis set are used for Pd. [d] Bridging Cl atom. $CF_2Cl-PdCl$ has a C_s structure in its singlet ground state, whereas $CFCl_2-PdCl$ has a C_1 structure with a bridging Cl atom.

47 and 41 kcal/mol more stable than the reactants. However, no absorptions from the insertion complex are observed. Normally the higher-oxidation-state complexes are relatively more stable in the matrix than predicted for the isolated molecules, probably due to more polarized bonds from the matrix interaction.[5−10] One other possibility is that the strong CCl_2 symmetric and antisymmetric stretching bands predicted at ~800 and ~770 cm^{-1} for the insertion product are covered by the strong precursor absorptions in the region of 820−740 cm^{-1}, and other absorptions are too weak to observe.

Pd + $CFCl_3$ and CF_2Cl_2. Figure 2 shows the spectra from reactions of Pd with $CFCl_3$ and CF_2Cl_2. In the Pd + $CFCl_3$ spectra both **m** and **i** absorptions are observed. The **m** absorptions remain unchanged on visible irradiation but more than triple on UV photolysis, increase slightly further on full arc photolysis, and decrease relatively fast in the process of annealing. The **i** absorptions also remain unchanged on visible photolysis, quadruple on UV irradiation, increase slightly on full arc photolysis, and sharpen first and then decrease on successive annealings.

The two **m** absorptions at 1261.3 cm^{-1} (with shoulders at 1259.7 and 1254.7 cm^{-1}) and at 991.2 cm^{-1} in the C−F and C−Cl stretching regions[10a,12] strongly indicate that the major product has a CFCl moiety, and the frequencies are well reproduced by calculations of the Pd carbene, $CFClPdCl_2$. The good agreement between the observed and calculated values as shown in Table 2 substantiate the formation of $CFClPdCl_2$, whose other bands are predicted to be too weak to observe here. The **i** absorptions at 1124.2, 900.4, and 602.2 cm^{-1} are assigned to the C−F, C−Cl, and C−Cl (bridging) stretching modes of $CFCl_2-PdCl$, and they also show reasonably good correlation with the DFT-calculated frequencies.

In the CF_2Cl_2 reaction product spectra, only **i** absorptions are observed, unlike the cases of CCl_4 and $CFCl_3$. The **i** absorptions dramatically increase upon UV photolysis (more than 500%) and increase further on full arc photolysis. The two strong **i** absorptions at 1199.0 and 1182.3 cm^{-1} (with a shoulder at 1183.9 cm^{-1}) in the C−F stretching region are assigned to the CF_2 symmetric and antisymmetric stretching absorptions of the insertion complex, $CF_2Cl-PdCl$. The observed frequencies are compared with the DFT frequencies in Table 3. The weaker **i** absorptions at 692.7 and 630.3 cm^{-1} are assigned to the CF_2 bending and wagging mode. The four observed bands are in fact the observably strong ones originating from the $CF_2Cl-PdCl$, as shown in Table 3. The four product absorptions, whose frequencies correlate well with the predicted frequencies, support formation of the C−Cl insertion complex in reaction of Pd with CF_2Cl_2.

The energy difference between the insertion and methylidene complexes gradually increases with fluorine substitution.

Table 4. Calculated Fundamental Frequencies of $CHCl_2$−PdCl Isotopomers in the ^1A Ground State[a]

approximate description	$CHCl_2$−PdCl obsd[b]	B3LYP[c]	int[c]	BPW91[c]	int[c]	$CDCl_2$−PdCl obsd[b]	B3LYP[c]	int[c]	BPW91[c]	int[c]
A′ C−H str.		3169.3	5	3095.3	4		2332.2	3	2277.5	2
A″ HCCl bend		1238.7	22	1189.2	20	923.8	925.1	83	888.2	93
A′ HCPd bend	980.1	1015.3	52	967.6	51	795.9	811.5	82	783.1	98
A″ CCl_2 asym. str.	729.2	793.6	156	773.5	179	709.8	737.6	59	712.8	52
A′ CCl_2 sym. str.	586.4	614.6	36	603.9	17	568.5	589.6	64	568.4	41
A′ C−Pd str.	542.2, 530.2	537.8	62	495.0	70	509.4, 495.6	504.8	28	472.0	44
A′ Pd−Cl str.		355.2	45	358.8	40		355.2	45	358.7	40
A′ CPdCl2 deform		298.8	2	287.8	3		297.1	2	286.2	3
A′ PdCCl bend		185.5	1	194.1	1		185.2	1	193.7	1
A″ C−Cl bend		172.0	3	167.4	2		170.9	3	166.4	2
A′ Pd−Cl tort.		69.8	2	76.3	1		69.6	2	75.9	1
A″ CPdCl bend		64.4	6	66.1	4		64.2	6	66.0	4

[a] Frequencies and intensities are in cm^{-1} and km/mol. [b] Observed in an argon matrix. [c] Frequencies and intensities computed with B3LYP or BPW91/6-311++G(3df, 3pd) are for harmonic calculations, and the SDD core potential and basis set are used for Pd. $CHCl_2$−PdCl has a C_s structure in the ground singlet state.

Note that CCl_3−PdCl and CCl_2−$PdCl_2$ have almost the same energy as described above; $CFCl_2$−PdCl and CFCl−$PdCl_2$ are 44 and 42 kcal/mol lower than the reactants (Pd(^{1}S) + $CFCl_3$), and CF_2Cl−PdCl and CF_2−$PdCl_2$ are 40 and 38 kcal/mol lower than the reactants (Pd(^{1}S) + CF_2Cl_2)). The present results reveal that the insertion complex is favored with increasing number of F atoms in reactions of Pd, consistent with the variation in the predicted energy difference between the insertion and methylidene complexes. CCl_4 produces exclusively CCl_2−$PdCl_2$, $CFCl_3$ forms both the insertion and methylidene products, and CF_2Cl_2 generates only the insertion complex CF_2Cl−PdCl.

This indicates that Cl migration from C to Pd following the initial C−Cl bond insertion becomes less favorable with the number of F substituents as the insertion complex becomes gradually more stable relative to the methylidene product.

Pd + $CHCl_3$. Figure 3 shows product absorptions from reactions of Pd with $CHCl_3$ and its deuterated isotopomer. Only **i** absorptions are observed parallel to the case of Ni + $CHCl_3$, which double on UV irradiation. The **i** absorption at 980.1 cm^{-1} has its D counterpart at 795.9 cm^{-1} (H/D ratio of 1.231) and is assigned to the HCPd bending mode of $CHCl_2$−PdCl on the basis of the frequency and large D shift. The product absorptions at 729.2 and 586.4 cm^{-1} show relatively small D shifts of 19.4 and 17.9 cm^{-1} (H/D ratio of 1.027 and 1.031), and they are assigned to the antisymmetric and symmetric stretching modes. The **i** absorption at 542.2 cm^{-1} (with a satellite at 530.2 cm^{-1}) has its D counterpart at 509.4 cm^{-1} (with a satellite at 495.6 cm^{-1}) (H/D ratio of 1.041), and it is assigned to the C−Pd stretching mode. Another **i** absorption at 923.8 cm^{-1} in the D spectra is assigned to the HCCl bending mode, while the H counterpart is believed to be covered by precursor absorption. The observed **i** absorptions showing a good correlation with the DFT frequencies (Table 4) without **m** absorptions reveal exclusive formation of the insertion complex in reaction of the group 10 metal with $CHCl_3$.

Pd + CH_2FCl and CH_2F_2. Figure 4 shows the product absorptions from reactions of Pd with CH_2FCl and CH_2F_2. Only **i** absorptions in the CH_2FCl spectra are observed again, which decrease slightly on visible irradiation but quadruple on UV irradiation. They increase slightly more on full arc photolysis (~500% increase in total) and sharpen in the early stage of annealing. The **i** absorption at 1191.5 cm^{-1} is assigned to the CH_2 wagging mode of the insertion complex, CH_2F−PdCl, the strong product absorption at 1008.1 cm^{-1} (with a shoulder at 1010.1 cm^{-1}) to the C−F stretching mode, and the weak **i** absorption at 598 cm^{-1} to the C−Pd stretching mode. The product absorptions correlate very well with the predicted frequencies for the insertion complex, as shown in Table 5.

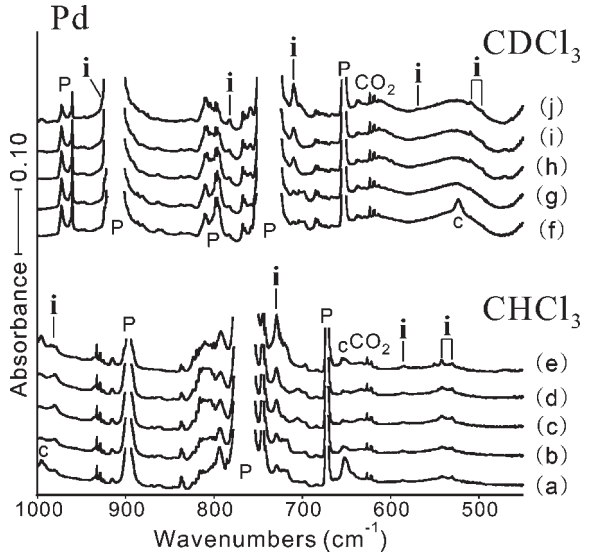

Figure 3. Infrared spectra in the 1000−450 cm^{-1} region for the reaction products of the laser-ablated palladium atom with chloroform isotopomers in excess argon at 10 K. (a) Pd and $CHCl_3$ (0.5% in argon) co-deposited for 1 h, (b−e) as (a) spectra taken following the irradiation and annealing sequence described in Figure 1 caption (visible, UV, and full arc irradiations and annealing to 26 K). (f) Pd and $CDCl_3$ (0.5% in argon) co-deposited for 1 h, (g−j) as (f) spectra taken following the same irradiation and annealing sequence. **i**, P, and c stand for product, precursor, and common absorptions, respectively.

The **i** absorptions in the CH_2F_2 spectra are much weaker and show only a small increase on UV photolysis, consistent with the general trend that substitution of Cl with F reduces reactivity toward transition metal atoms.[5−10] The product absorptions at 1205.4, 989.7, and 506 cm^{-1} are attributed to the CH_2 wagging, C−F stretching, and C−Pd stretching modes of CH_2F−PdF, and the observed frequencies are compared with the DFT values in Table 5.

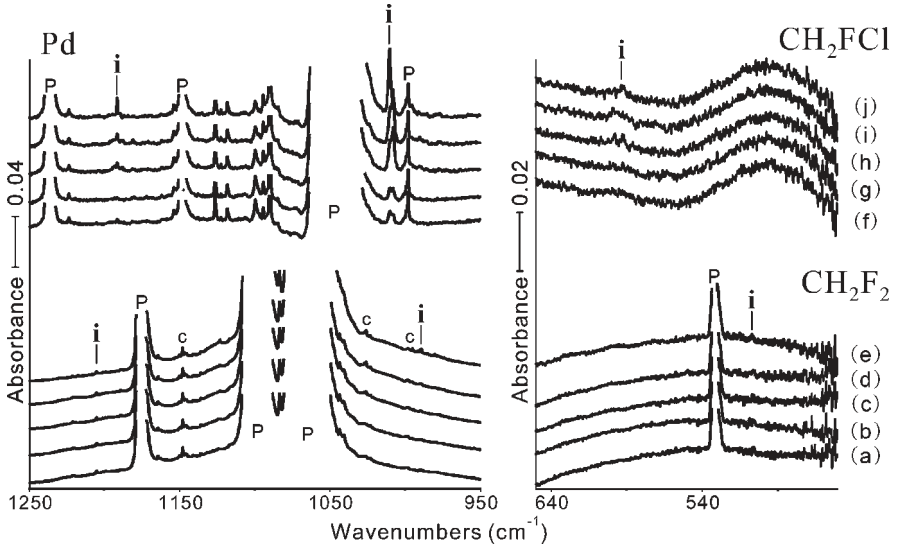

Figure 4. Infrared spectra in the 1250−950 and 650−450 cm^{-1} regions for the reaction products of the laser-ablated palladium atom with CH_2F_2 and CH_2FCl in excess argon at 10 K. (a) Pd and CH_2F_2 (0.5% in argon) co-deposited for 1 h, (b−e) as (a) spectra taken following the irradiation and annealing sequence described in Figure 1 caption (visible, UV, and full arc irradiations and annealing to 26 K). (f) Pd and CH_2FCl (0.5% in argon) co-deposited for 1 h, (g−j) as (f) spectra taken following the same irradiation and annealing sequence. **i**, P, and c stand for product, precursor, and common absorptions, respectively.

Table 5. Observed and Calculated Fundamental Frequencies of CH_2F-PdF and $CH_2F-PdCl$ in the ^1A Ground States[a]

	CH_2F-PdF						$CH_2F-PdCl$				
approximate description	obs[b]	B3LYP[c]	int[c]	BPW91[c]	int[c]	approximate description	obs[b]	B3LYP[c]	int[c]	BPW91[c]	int[c]
A″ CH_2 asym. str.		3173.5	1	3099.4	2	A″ CH_2 asym. str.		3180.9	1		
A′ CH_2 sym. str.		3068.2	9	2993.3	10	A′ CH_2 sym. str.		3075.0	8		
A′ CH_2 scis.		1465.4	0	1413.6	0	A′ CH_2 scis.		1468.0	1		
A′ CH_2 wag	1205.4	1217.8	47	1168.6	38	A′ CH_2 wag	1191.5	1218.2	49		
A″ CH_2 twist		1175.2	4	1134.6	3	A″ CH_2 twist		1185.8	3		
A′ C−F str.	989.7	1003.9	206	964.1	182	A′ C−F str.	1010.1, 1008.1	1004.0	255		
A″ CH_2 rock		756.3	6	728.1	5	A″ CH_2 rock		755.8	4		
A′ Pd−F str.		625.6	22	614.4	24	A′ C−Pd str.	598	618.1	20		
A′ C−Pd str.	506	535.0	73	528.8	61	A′ Pd−Cl str.		349.5	27		
A′ FCPd bend		237.6	1	233.7	1	A′ FCPd bend		227.9	4		
A″ CPdF oop. bend		96.0	12	94.7	10	A′ CPdCl bend		88.8	9		
A′ CPdF ip. bend		87.6	20	97.8	17	A″ CH_2F tort.		83.0	8		

[a] Frequencies and intensities are in cm^{-1} and km/mol. [b] Observed in an argon matrix. [c] Frequencies and intensities computed with B3LYP or BPW91/6-311++G(3df, 3pd) are for harmonic calculations, and the SDD core potential and basis set are used for Pd. $CH_2F-PdCl$ and $CH_2F-PdCl$ have a C_s structure in the ground singlet state.

Structure and Bonding in Pd Complexes. The structures of the identified Pd complexes in this study are illustrated in Figure 5. The Pd carbenes, CCl_2-PdCl_2 and $CFCl-PdCl_2$, have staggered allene-type structures in their singlet ground states, and CF_2-PdCl_2, while not identified in the spectra, is calculated to have a similar structure. The methylidene C−Pd bond lengths of 1.825, 1.823, and 1.835 Å (B3LYP) and 1.779, 1.778, and 1.785 Å (CASPT2) are compared with C−Pd bond lengths of 1.86−2.08 Å for Pd carbene complexes.[26] The CASPT2 structures are shown in Figure 6.

Parallel to the Ni and Pt cases, the Pd carbene C−Pd bonds are essentially double bonds: the effective C−Pd bond orders (EBO) from CASPT2 analysis (bonding minus antibonding occupancies divided by 2) of CCl_2-PdCl_2, $CFCl-PdCl_2$, and CF_2-PdCl_2 are 1.89, 1.90, and 1.92. The CASPT2 molecular orbitals involved in the C=Pd bonds are illustrated in Figure 7. In order to have a fair comparison among the group 10 metal carbenes, CASPT2 calculations were also done for the analogous Pt carbenes, and the structures and molecular orbitals are shown in Figures S1 and S2 (Supporting Information). Note that the EBO for CCl_2-PtCl_2, $CFCl-PtCl_2$, and CF_2-PtCl_2 are 1.89, 1.90, and 1.91, and recall that the analogous values for the Ni carbenes are 1.81, 1.84, and 1.87.[12] It is interesting to find that the CASPT2 bond lengths for the C=M double bonds are nearly the same for the CCl_2-MF_2 (Ni, 1.686 Å; Pd, 1.790 Å; Pt, 1.783 Å) and the CF_2-MCl_2 structural isomers (Ni, 1.658 Å; Pd, 1.785 Å; Pt, 1.782 Å).

The CASPT2 EBO values show that for CCl_2-MCl_2, $CFCl-MCl_2$, and CF_2-MF_2 there is a very slight increase in EBO on going down the group 10 family as the heavier Pd and Pt metals appear to form more effective (p−d)π bonds than Ni. Parallel to the Ni and Pt cases, the F atom on the

(26) Kremzow, D.; Seidel, G.; Lehmann, C. W.; Fürstner, A. *Chem.—Eur. J.* **2005**, *11*, 1833. (b) Wang, C.-Y.; Liu, Y.-H.; Peng, S.-M.; Chen, J.-T.; Liu, S.-T. *J. Organomet. Chem.* **1997**, *532*, 261. (c) Weng, W.; Chen, C.-H.; Foxman, B. M.; Ozerov, O. V. *Organometallics* **2007**, *26*, 3315 (C−Pd length).

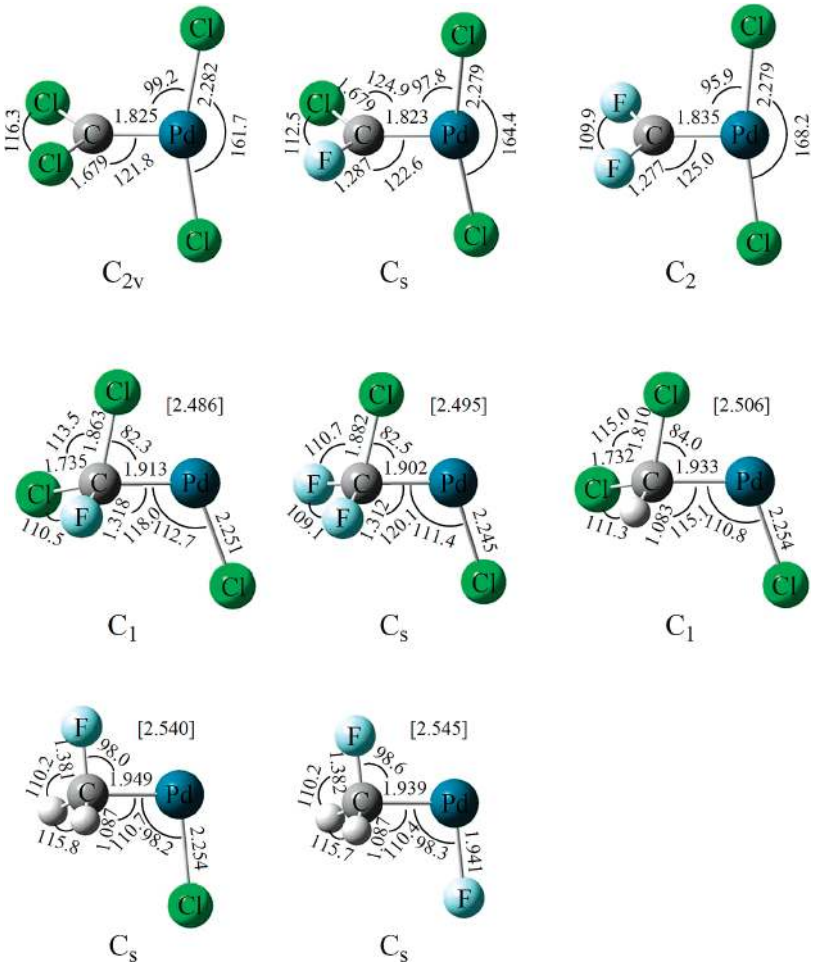

Figure 5. Structures calculated for the identified reaction products of palladium with halomethanes at the B3LYP level of theory using the 6-311++G(3df,3pd) basis sets for C, F, and Cl and SDD pseudopotential and basis set for Pd. Bond distances and angles are in Å and deg. Molecular symmetries are given under each structure. Notice the allene-type structures of the Pd methylidenes and the bridged structures of the insertion complexes [the bridged halogen−metal distance is given in brackets].

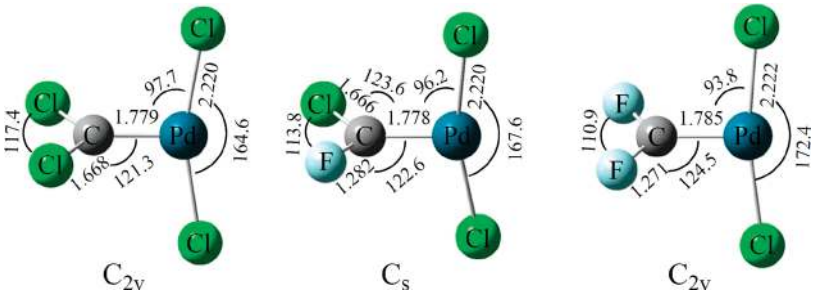

Figure 6. Calculated CASPT2 structures for three palladium carbenes.

carbon atom leads to a higher effective bond order probably because the more electronegative F contracts carbon 2p-orbitals and makes more effective overlap for bond formation.[10a,12]

Among the insertion complexes, $CFCl_2$−PdCl, CF_2C−PdCl, and $CHCl_2$−PdCl have bridged structures, whereas CH_2F−PdCl and CH_2F−PdF do not. Evidently coordination of the Cl electrons to the metal center is more effective than that of the F or H electrons, parallel to the Fe and Ni systems.[8,10]

Reactions. Previous studies and the present results reveal that high-oxidation-state complexes are generated from reactions of group 3−10 transition metals and actinides with small alkanes and halomethanes.[5−10,27] However, the preference for methylidene products in reactions of group 10 metals varies substantially. Pt, which is regarded in general as the strongest insertion agent among group 10 metals,[13] forms carbenes in methane and haloalkane reactions.[10] The Ni carbene complexes are, on the other hand, far less favored.[12] They are produced only in reactions with tetrahalomethanes, owing to the preference of the M−X bond

(27) Cho, H.-G.; Andrews, L. *Reactions of group 9 metals with halomethanes*, unpublished data.

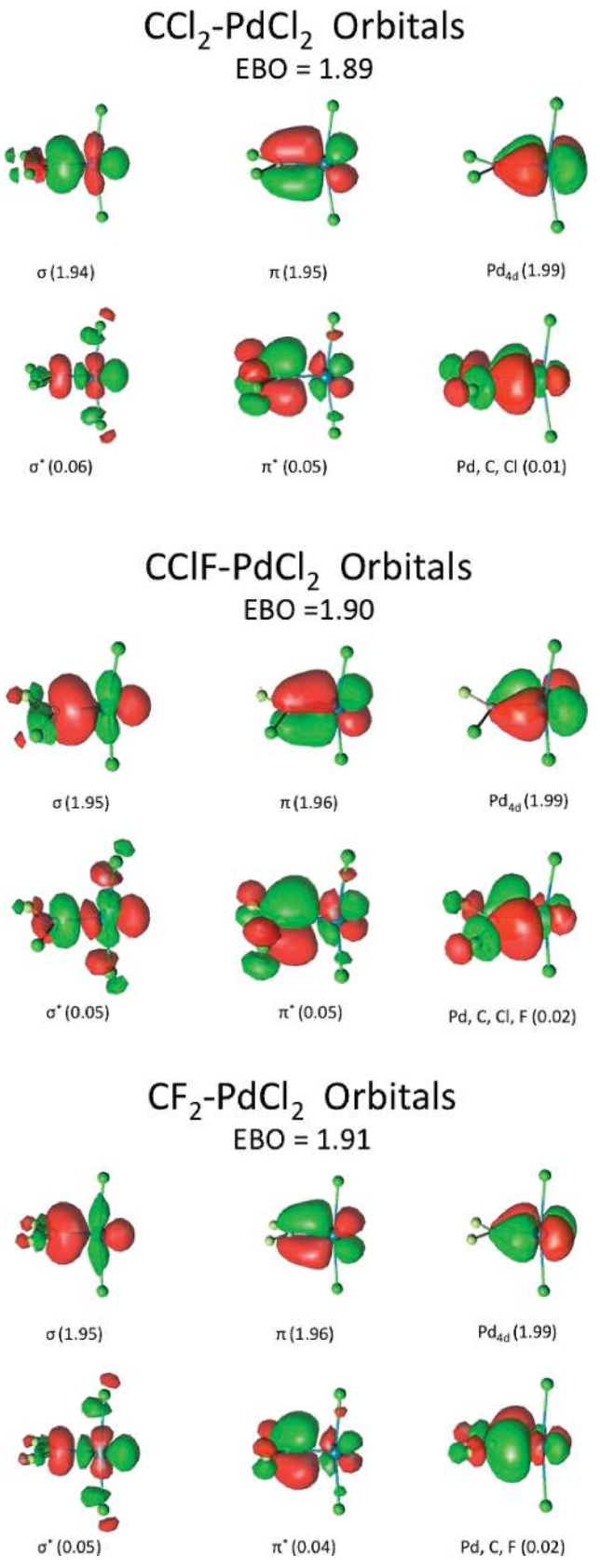

Figure 7. Calculated CASPT2 orbitals involved in the carbon−palladium double bonds.

(particularly M−Cl bond) over the M−H bond. Only the insertion complex is formed with other precursors. These results suggest that group 10 metals are the limit for generating the carbene complex in reactions with small alkanes and halomethanes, which is consistent with the fact that Ni carbene complexes are rare.[2]

Pt gives far stronger carbene product absorptions.[10a] On the basis of the similar calculated CCl_2 stretching absorption intensities for the group 10 metal methylidenes,[10,12] Pt is at least 3 times more reactive than Ni and Pd. For Ni and Pd, in the original spectra the Ni methylidene absorptions are twice as strong as the Pd counterparts. However, Pd has strong absorption in the UV region,[28] resulting in a dramatic increase of the methylidene product absorptions, presumably through photoactivation of the Pd reaction with CX_4. After the process of photolysis the Pd methylidene absorptions are almost twice as strong as the Ni methylidene absorptions. In all Pd spectra, the product absorptions triple or quadruple on UV irradiation.

Recent investigation in our laboratory has shown that laser-ablated transition metal atoms react with halomethanes through C−X bond activation/insertion followed by α−X transfer,[8,9] reaction 1. The Pd oxidative insertion reaction into C−X bonds has been explored by density functional theory:[4c] direct insertion into the C−X bond occurs in the gas phase reaction, which becomes easier on going down the halogen family column. This is in agreement with the present experimental observations.

$$M^* + CX_4 \rightarrow CX_3{-}MX^* \rightarrow CX_2{-}MX_2^* \rightarrow CX{-}MX_3 \quad (1)$$

The present results reveal that C−X bond insertion by group 10 metal atoms occurs in reactions with halomethanes, and in the case of tetrahalomethanes, X migration from C to M also follows. However, further X migration to form the carbyne product has not been observed, owing to the much higher energy of the product. The carbyne $CCl{-}PtCl_3$ is computed to be 27 kcal/mol higher energy than $CCl_2{=}PtCl_2$,[10a] and geometry optimizations for $CCl{-}NiCl_3$ and $CCl{-}PdCl_3$ result in the corresponding carbene complexes.

Conclusions

Laser-ablated Pd atoms react with halomethanes, and the products are identified on the basis of isotopic shifts and correlation with DFT-computed frequencies. The $CX_2{=}PdX_2$ molecules are produced by reactions with tetrahalomethanes, analogous to Pt and Ni,[10,12] while the reaction is more exothermic and the yield much higher for X = Cl than X = F. On the other hand, only insertion complexes are identified from reactions with precursors containing H, indicating that X migration from C to M following initial C−X bond insertion becomes more difficult. This also suggests that group 10 metals mark the limit where carbene complexes are no longer produced in transition metal reactions with halomethanes. The carbon−metal bonds in the Ni, Pd, and Pt carbenes are essentially double bonds with CASPT2 effective bond orders in the 1.8 to 1.9 range. The CASPT2 EBO values for $CCl_2{-}MCl_2$ and $CFCl{-}MCl_2$ show a very slight increase on going down the group 10 family, but for the more heavily fluorine-substituted species $CF_2{-}MF_2$, this trend is reversed.

(28) Klotzbucher, W.; Ozin, G. A. *Inorg. Chem.* **1976**, *15*, 292.

Evidence shows that the small group 10 metal complexes have singlet ground states. While singlet states are clearly the most stable for the identified Pd and Pt complexes, DFT calculations suggest that singlet and triplet states for the Ni complexes have nearly the same energies.[10,12] However, the observed vibrational characteristics show that most of the Ni products also have singlet ground states. The simple Pd carbene complexes all have staggered structures, whereas the insertion products with the C−Cl bond assume bridged structures, indicative of efficient Cl electron donation to the metal center.

Acknowledgment. We gratefully acknowledge financial support from National Science Foundation (U.S.) Grant CHE 03-52487 to L.A. and support from Korea Institute of Science and Technology Information (KISTI) by Grant No. KSC-2008-S02-0001 and from the Swiss National Science Foundation (Grant 200020-120007).

Supporting Information Available: Figures S1 and S2 of CASPT2 structures and C=Pt molecular orbitals for Pt carbenes. This material is available free of charge via the Internet at http://pubs.acs.org.